International Journal of Heat and Fluid Flow 30 (2009) 276–285

Contents lists available at ScienceDirect

International Journal of Heat and Fluid Flow

journal homepage: www.elsevier.com/locate/ijhff

Experimental study and large eddy simulation for the turbulent flow around four cylinders in an in-line square configuration

K. Lam [a,*], L. Zou [b]

[a] Department of Mechanical Engineering, The Hong Kong Polytechnic University, Hung Hom, Kowloon, Hong Kong
[b] School of Mechanical and Electronic Engineering, Wuhan University of Technology, Wuhan 430070, China

ARTICLE INFO

Article history:
Received 23 February 2007
Received in revised form 15 January 2009
Accepted 16 January 2009
Available online 23 February 2009

Keywords:
Four cylinders
Turbulent flow
LDA
DPIV
LES

ABSTRACT

The turbulent flows around four cylinders in an in-line square configuration with different spacing ratios of 1.5, 2.5, 3.5 and 5.0 have been investigated experimentally at subcritical Reynolds numbers from 11,000 to 20,000. The mean and fluctuating velocity distributions were obtained using the laser Doppler anemometry (LDA) measurement. The digital particle image velocimetry (DPIV) was employed to characterize the full field vorticity and velocity distributions as well as other turbulent quantities. The experimental study indicated that several distinct flow patterns exist depending on the spacing ratio and subcritical Reynolds number for turbulent flow. The three-dimensional numerical simulations were also carried out using the large eddy simulation (LES) at Reynolds number of 15,000 with the spacing ratio of 1.5 and 3.5. The results show that the LES numerical predictions are in good agreement with the experimental measurements. Therefore, the three-dimensional vortex structures and the full field instantaneous and mean quantities of the flow field such as velocity field, vorticity field, etc., which are very difficult to obtain experimentally, can be extracted from the simulation results for the deepening of our understanding on the complex flow phenomena around four cylinders in in-line configuration.

1. Introduction

The wake interference around the cylinder arrays have been widely investigated in the past because of its inherent important and practical significance in many engineering applications. More recent research include works by Norberg (1998), Sumner et al. (2000), Park and Lee (2003), Wang and Zhou (2005), Deng et al. (2006) and Carmo and Meneghini (2006). Most of the experimental and numerical investigations are concentrated on flows around one or two cylinders. The more complex wake flow around four-cylinder arrays configuration has not been studied as extensively as the single and two cylinders configurations. However, a number of studies of the fluid dynamics for the four-cylinder arrays can still be found.

Sayers (1988, 1990) conducted experiments on four cylinders in square configurations with two end-plates in the spacing ratio range of 1.5–5 with an aspect ratio of 11.5 at the Reynolds number of 30,000. Lam and Lo (1992) and Lam and Fang (1995) experimentally investigated the force and pressure characteristics of turbulent flow around four cylinders in square configurations. The relationship between force and spacing ratio was obtained. With the spacing ratio less than 1.7, the bistable feature behind the downstream cylinders was observed. The regular shedding behind the upstream cylinders is suppressed with the spacing ratio less that 3.94 at Reynolds number of 2100. Further increasing the spacing ratio, the vortex shedding becomes steady and regular. Farrant et al. (2000) numerically captured the two-dimensional laminar flow characteristics and interactive forces associated with flows around four equi-spaced cylinders at a Reynolds number of 200 using a cell boundary element method. Lam et al. (2003a,b) carried out extensively experimental investigations using laser induced fluorescent (LIF) visualization and particle image velocimetry (PIV) techniques for the cross-flow around four cylinders in different spacing ratios and different orientations at different Reynolds numbers. Furthermore, the numerical investigations on the four-cylinder arrays were also carried out by Lam and Zou (2006) and Lam et al. (2008) at the laminar flow condition. By using the finite-volume method (FVM), the two- and three-dimensional simulations were performed at a Reynolds number of 200. Some typical wake behaviour around the four cylinders was predicted accurately. The complex three-dimensional wake structures were captured using the 3D simulations. The force and pressure coefficients distributions as well as the transformation of the flow patterns around the four cylinders were obtained. However, the quantitative data of the velocity distributions, the instantaneous vorticity fields, the complex three-dimensional vortex structures and the Reynolds stress etc. for the turbulent flow around four cylinders in an in-line square configuration at subcritical Reynolds number are still not available.

* Corresponding author. Tel.: +852 2766 6649; fax: +852 2365 4703.
E-mail address: mmklam@polyu.edu.hk (K. Lam).

0142-727X/$ - see front matter © 2009 Elsevier Inc. All rights reserved.
doi:10.1016/j.ijheatfluidflow.2009.01.005

The present study focuses attention on the complex turbulent wake formed by the four cylinders in an in-line square configuration. The main objectives of the present study are to investigate in detail the effects of the spacing ratio and the Reynolds number on the mean and fluctuating velocity distributions, the complex vorticity field and the flow patterns around the four cylinders in an in-line square configuration at subcritical Reynolds number ranging from 11,000 to 20,000 with the spacing ratio of 1.5, 2.5, 3.5 and 5.0. Advanced experimental methods such as laser Doppler anemometer (LDA) and digital particle image velocimetry (DPIV) techniques were employed to acquire the quantitative data. However, due to the difficulties in experimental measurements in certain positions and configurations, numerical simulation results for such complex turbulent flow were sought. In order to capture the detailed three-dimensional vortex structures and obtain the full field instantaneous and mean physical information such as the mean and fluctuating pressure, forces and the vortex-shedding characteristics as well as the Reynolds stresses, the 3D numerical simulations of the turbulent flows around the four cylinders in an in-line square configuration with the spacing ratio of 1.5 and 3.5 were carried out using the large eddy simulation (LES) at the Reynolds number of 15,000. The purposes of comparison for numerical and experimental results could lead to a better understanding of the effects of wake interference of the turbulent flows around the four cylinders in an in-line square configuration. Moreover, the validity of the LES numerical simulation in the prediction of the complex turbulent flows around the four cylinders is examined. A proper and accurate numerical simulation would thus reduce the works of the costly and complicated experimental measurements in the investigation of the complex turbulent wake flows.

2. Experiment details

2.1. Experimental setup

The experimental investigation on turbulent flow around four cylinders in an in-line square configuration was carried out using a closed-circuit water tunnel with a working square cross-section of 0.3 m $\times$ 0.6 m and a length of 2.4 m (see Fig. 1a). The four circular acrylic cylinders of diameter D = 20 mm were placed horizontally with two moveable end-plates at the mid of the water tunnel. As shown in Fig. 1b, for schematic diagram of experimental system for the four cylinders in in-line square configuration and the definition of the coordinate system.The origin of the coordinate system is located at the centre point of the four cylinders arrangement with (x, y, z) denoting the coordinates along the streamwise x-direction, the transverse y-direction and the spanwise z-direction

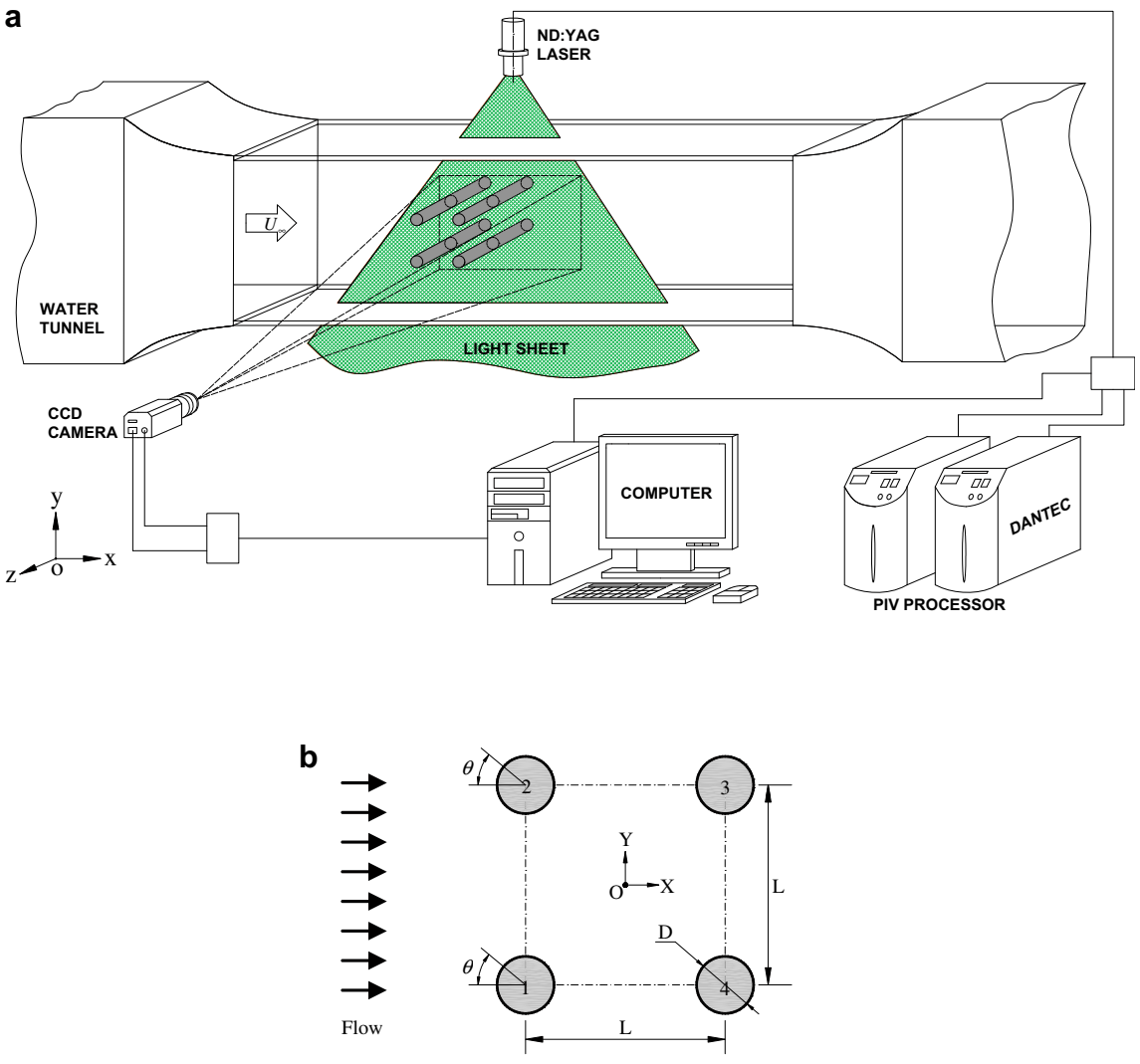

Fig. 1. Schematic diagram of experimental setup for the four cylinders in in-line square configuration.

of the cylinder, respectively. The spacing ratio (L/D) is set at 1.5, 2.5, 3.5 and 5.0 with an aspect ratio (H/D) of 20. This leads to a blockage ratio (per cylinder) of ~5%. The incoming flow velocity U_∞ was adjusted to 0.55, 0.75 and 1.00 m/s, corresponding to the Reynolds number of 11,000, 15,000 and 20,000, respectively. At U_∞ = 0.55 m/s, the boundary layer on the wall was found to be less than 20 mm thick, while the free-stream turbulent intensity was measured to be less than 2%.

2.2. LDA measurement

In order to obtain the quantitative mean and fluctuating velocity distributions for turbulent flow around the four cylinders, a two-colour fibre-optic LDA (Dantec Model 58N40 LDA with enhanced FVA signal processor) was employed in the present investigations. The LDA system is equipped with software for data processing and analysis. The LDA measuring volume has a minor axis 1.18 mm and a major axis of 2.48 mm. Thus, experimental uncertainties are estimated to have an error <2% in mean velocity and a corresponding error <5% for the root mean square values. The LDA measurements were carried out at difference streamwise positions of the flow field. For each data-point, 50,000 validated samples were acquired with a data rate of 0.8–4 kHz.

2.3. DPIV measurement

The Dantec standard DPIV system was used to measure the instantaneous vorticity fields and velocity distributions. The flow was seeded by 20 μm polyamide particles with the density of 1.03 g/cm^3. The flow field was illuminated by two Nd:Yag pulsed laser sources with a wavelength of 532 nm, each cavity having a maximum energy output of 120 mJ. The flow images were captured using a CCD camera (HiSense type 13, double frames, gain ×4, 1280 × 1024 pixels). A Dantec FlowMap Process (type PIV2001) was used to calculate the raw displacement vector field from the particle image data. The measurement was conducted at the mid-span of the cylinders. The observation area covered about 210 mm × 210 mm at the L/D = 3.5 case and varied correspondingly according to L/D. In image processing, the interrogation window consisted of 32 × 32 pixels with a 50% overlap in either of the two directions, corresponding to 79 × 63 velocity vectors. A total of 200 PIV images were obtained for each measurement. Time-averaged patterns of the flow structure were calculated from all of the instantaneous images. The LDA and DPIV systems were introduced in detail by Lam et al. (2004).

3. Computational models

3.1. Governing equations

By using the three-dimensional LES turbulence model, the large-scale eddies are solved directly by the filtered Navier–Stokes equations and the small eddies are modeled using a subgrid scale (SGS) model. The governing equations employed for LES are

$$\frac{\partial \overline{u}_i}{\partial x_i} = 0, \tag{1}$$

$$\frac{\partial \overline{u}_i}{\partial t} + \frac{\partial \overline{u}_i \overline{u}_j}{\partial x_j} = -\frac{1}{\rho}\frac{\partial \overline{p}}{\partial x_i} + \nu \frac{\partial^2 \overline{u}_i}{\partial x_j \partial x_j} - \frac{\partial \tau_{ij}}{\partial x_j}, \quad (i = 1,2,3), \tag{2}$$

where $\overline{u}_i$ are the filtered velocity components along the Cartesian coordinates x_i, $\overline{p}$ is the pressure, ρ is the fluid density and ν is the kinematic viscosity of the fluid. The influence of the small scales on the large (resolved) scales takes place through the subgrid scale stress defined by

$$\tau_{ij} = \overline{u_i u_j} - \overline{u}_i \overline{u}_j, \tag{3}$$

resulting from the filtering operation, which are unknown and must be modeled with a subgrid model. All computations in the present work were carried out with a Smagorinsky constant of C_s = 0.1. (The detailed description can be found in Lam and Lin (2008).)

3.2. Numerical method

In the present simulation, the finite-volume method (FVM) applied on unstructured grids is employed to calculate the three-dimensional unsteady incompressible Navier–Stokes equation. A second-order central differencing scheme is used for momentum discretization while a second-order implicit scheme is employed to advance the equations in time. The well-known pressure implicit method with splitting of operators (PISO) algorithm is used to deal with the pressure–velocity coupling between the momentum and the continuity equations.

3.3. Computational domain and boundary conditions

Similar to the experimental setup, in the computational domain, the origin of the coordinate system is located at the centre point of the four-cylinder arrangement with the (x,y,z) denoting the coordinates along the streamwise x-direction, the transverse y-direction and the cylinder spanwise z-direction, respectively. The computational domain in the x- and y-directions are set at 32D and 20D, respectively. The upstream boundary is set at 8D away from the coordinate origin and the downstream boundary is 24D away from the origin. The experimental studies of Williamson et al. (1995) and Williamson (1996) showed that the wavelength of the streamwise vortex structures in the near wake of a circular cylinder scales is given by $\lambda_z/D \approx 25Re^{-1/2}$. Further downstream, the large-scale structure for streamwise vortices has a wavelength $\lambda_z/D \approx 1$. Here λ_z is the spanwise wavelength of the vortices. In the present simulations, the Reynolds number is fixed at $Re = U_\infty D/\nu$ = 15,000 for all the cases studied. So the estimated $\lambda_z/D \approx 0.2$. The computational domain in the z-direction is set at 3D, which will fulfill with the present simulations.

Fig. 2 shows that the computational domain is divided into a number of unstructured hexahedral grids. On the x–y plane, the grid is not uniform but uniform along the z-direction. The grid is clustered near the cylinder and the spacing is increased with a

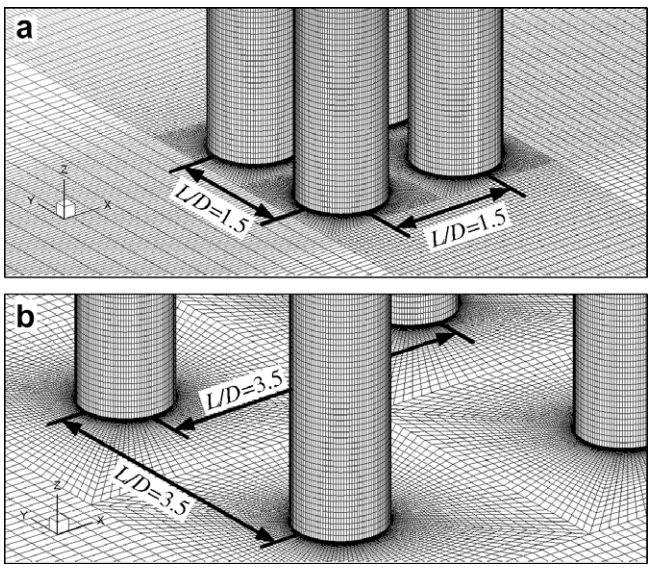

Fig. 2. Grid distributions around the four cylinders: (a) L/D = 1.5 and (b) L/D = 3.5.

ratio of 1.1 away from the cylinder. The distance from the cylinder surface to the nearest grid points are fixed at $y^+ = 1$. At the inlet boundary, a uniform velocity profile ($u = 1$, $v = w = 0$) is imposed, while the convective boundary condition $(\partial u_i/\partial t + U_c(\partial u_i/\partial x) = 0)$ is used at the outlet boundary [Breuer (1998), Sohankar et al. (2000), Lam and Lin (2008)], where U_c is the convection velocity equal to the mean velocity at the inlet. A periodic boundary condition is employed at the boundaries in the spanwise direction and a no-slip boundary condition ($u = v = w = 0$) is prescribed at the surface of the cylinders. The lateral surfaces are treated as slip surfaces using symmetry conditions ($\partial u/\partial y = \partial w/\partial y = v = 0$).

Initially, the grid independence tests were carried out considering that the accuracy of the computational results using LES is highly dependent on the mesh size and cell numbers. The grid number of 2.8×10^6 for the cylinders with $L/D = 1.5$ and 2.98×10^6 for $L/D = 3.5$, respectively, were adopted for the final results discussion (grid Model-C, in Table 1, the detailed grid independence and validation test will be discussed in the next section). A dimensionless time step $\Delta t U_\infty/D = 0.02$ was chosen for the simulation, yielding the maximum CFL number close to 2 and ensured sufficiently small CFL numbers less than 1 for most part of the computational domain. At least 200 dimensionless time units (tU_∞/D), which corresponded to about 40 vortex-shedding cycles, were taken so as to obtain more reliable statistical information. The overall drag coefficient is defined by $C_D = 2F_D/\rho U_\infty^2 DH$,while the overall lift coefficient is $C_L = 2F_L/\rho U_\infty^2 DH$. The total drag force and total lift force are given by F_D and F_L, respectively.

4. Results and discussion

4.1. Velocity distributions

Fig. 3 shows the normalized mean streamwise velocity (U/U_∞) distributions in the near wake of the four cylinders in an in-line square configuration with the spacing ratio (L/D) of 1.5, 2.5, 3.5 and 5.0 at the Reynolds numbers of 11,000, 15,000 and 20,000 obtained by the LDA measurement technique. The nondimensional distance (x/D) from the centre of the four cylinders configuration is different with the variation of spacing ratio L/D. At the position of $L/D = 1.5$ and $x/D = 2.25$ (Fig. 3a), as the increasing of Re, the level of asymmetry of the wake velocity profiles decreases. The minimum value of mean streamwise velocity varies from 0.25 to 0 in the $y/D = -0.75$ plane while it is always about -0.2 in the $y/D = 0.75$ plane when the Reynolds number varies from 11,000 to 20,000. It implies that the flow always in the reverse flow region behind the downstream cylinder of cylinder 3 (at the position of $x/D = 2.25$ and $y/D = 0.75$, refer to Fig. 1b). As a result, the vortex formation length (the location of the time-averaged closure point on the wake centreline ($U/U_\infty = 0$), similar to that defined by Lam et al. (2004) and Lam and Lin (2008)) is different behind the two downstream cylinders. This suggests that the flow structure behind the downstream cylinders is distinctly biased to one side

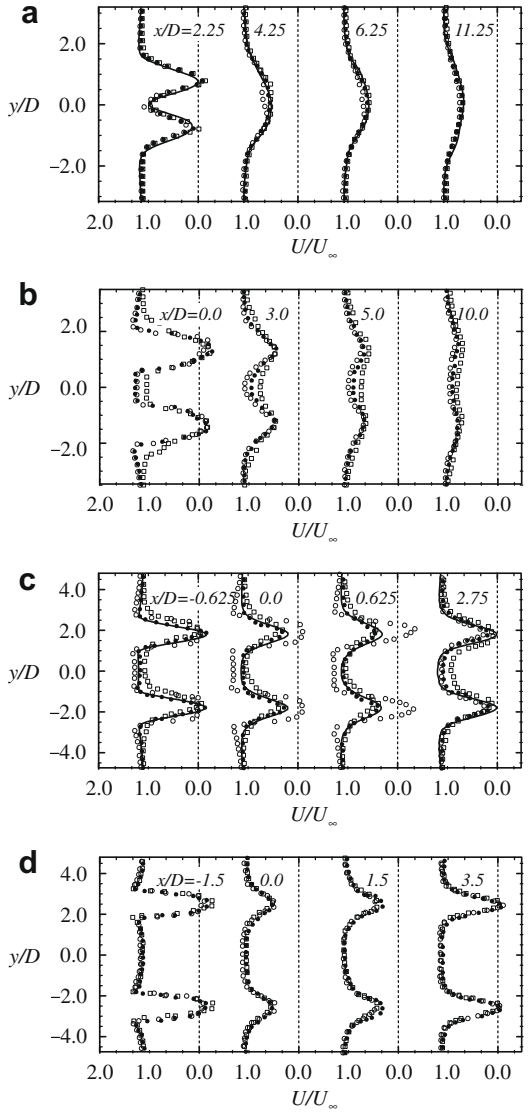

Fig. 3. Comparison of the mean streamwise velocity distributions derived from LDA measurements at different x-positions with different spacing ratios for (○) $Re = 11{,}000$, (●) $Re = 15{,}000$ and (□) $Re = 20{,}000$, (a) $L/D = 1.5$, (b) $L/D = 2.5$, (c) $L/D = 3.5$ and (d) $L/D = 5.0$. The solid line: LES results at $Re = 15{,}000$.

and it exhibits a bistable state (like that of the side-by-side cylinders, with a wide and narrow wakes behind the downstream cylinders, and the irregular changes of the wide and narrow wakes, as observed and discussed by Ng et al. (1997) and Wang and Zhou (2005)) for all the present Reynolds numbers. At further downstream positions from $x/D = 6.25$ to $x/D = 11.25$, the normalized mean streamwise velocity distributions indicate that the wake structure behind the downstream cylinders 3 and 4 forms an amalgamated structure with a single wide wake.

Fig. 3b shows the normalized mean streamwise velocity distributions with the spacing ratio of $L/D = 2.5$. Behind the two downstream cylinders (cylinders 3 and 4), the velocity distributions are basically not different for all the Reynolds numbers investigated in the present study. The values of mean streamwise velocity are negative at $x/D = 0$ behind the two upstream cylinders (cylinders 1 and 2). It suggests that the free shear layers from the upstream cylinders reattach or roll up very near the downstream cylinders and induces a reverse flow between the upstream and downstream cylinders. The wake structure behind the downstream cylinders is symmetrical with the central plane of $y/D = 0$. The

Table 1
Details of grid models for mesh-independence tests (Nc: the circumference mesh numbers; Nz: the cylinder spanwise mesh layers).

Grid	Cells	Nc	Nz	
Model-A	$L/D = 1.5$	1,224,000	100	32
	$L/D = 3.5$	1,327,200		
Model-B	$L/D = 1.5$	1,483,200	120	48
	$L/D = 3.5$	1,514,400		
Model-C	$L/D = 1.5$	2,781,600	160	48
	$L/D = 3.5$	2,980,800		

interference effect or amalgamation of wake regions with one another is not distinctively observed at further downstream positions.

Lam and Lo (1992) defined a critical spacing ratio for the shielding of the downstream cylinder by the upstream cylinder and found that it is around 3.94 at $Re = 2100$. Lam et al. (2003a) also observed that the downstream cylinders are completely shielded by their upstream cylinders for $L/D = 4$ at $Re = 200$. However, Lam et al. (2003b) showed that the critical spacing ratio is close to $L/D = 3.5$ at $Re = 41{,}000$ by experimental measurements. Recently, Lam et al. (2008) pointed out that the critical spacing ratio is very sensitive and occurs in the range of $L/D = 3.5$–4 for laminar flow condition. Therefore, the different results may due to the effect of the Reynolds numbers. Considering the discussion above, in the present investigation, for the critical spacing region corresponding to $L/D = 3.5$ (see Fig. 3c), at the position of $x/D = -0.625$, the values of mean streamwise velocity are negative (reaching about -0.2 and -0.1 for $Re = 15{,}000$ and 20,000, respectively) behind the upstream cylinders and in $x/D = 0$ and $x/D = 0.625$ planes, the values of U/U_∞ are positive at the $y/D = \pm 1.75$ planes for $Re = 15{,}000$ and 20,000. For $Re = 11{,}000$, however, the maximum reverse flow region occurs at $x/D = 0.625$ plane (reaching about $U/U_\infty = -0.4$) and the velocity values are approximately zero in the $y/D = \pm 1.75$ planes at $x/D = 0$ and -0.625 planes. It indicates that the flow behind the upstream cylinders is in the high reverse flow condition and vortex shedding from the upstream cylinders occurs for $Re = 15{,}000$ and 20,000 while the free shear layers of the upstream cylinders roll up to vortices just before the downstream cylinder and vortices are shed immediately downstream of cylinders 3 and 4 for $Re = 11{,}000$. Furthermore, it also suggests that there is a decrease in the vortex formation length behind the upstream cylinders as Re increases from 15,000 and 20,000. In $x/D = 2.75$ plane (the distance from the centre of the downstream cylinders is about $1D$), the value of U/U_∞ shows a decrease at the positions of $y/D = \pm 1.75$ as Re increases. It suggests that the wake formation regions of the downstream cylinders at the $Re = 11{,}000$ is shorter than that at higher Reynolds numbers. This could be due to the shear layer of the upstream cylinders rolled up very near the frontal part of the downstream cylinders at $Re = 11{,}000$, creating a more turbulent flow near the surfaces of the downstream cylinders and hence induces the shrinkage of the vortex formation region behind the downstream cylinders.

Fig. 3d shows that for $L/D = 5.0$, in $x/D = -1.5$, 0 and 1.5 planes, the normalized mean streamwise velocity distributions exhibit the similar phenomenon as that of $L/D = 3.5$ at $Re = 15{,}000$. It indicates that the flow behind the upstream cylinders is in the high reverse flow condition and exhibits a similar flow pattern where the free shear layers from upstream cylinders roll up into mature vortices and impinge on the downstream cylinder surfaces at such Reynolds number. It is interesting that the mean streamwise velocity distributions at $x/D = 3.5$ (the distance from the centre of the downstream cylinders is about $1D$) is very similar to that at $x/D = -1.5$ (the distance from the centre of the upstream cylinders is about $1D$). It is also close to that of a single cylinder at the similar Reynolds number and the results are consistent with the flow visualization results obtained by Lam and Lo (1992).

Fig. 4 shows that the mean transverse velocity (V/U_∞) distributions at $Re = 15{,}000$ with $L/D = 1.5$ and 3.5 also show the similar flow characteristics like that of the mean streamwise velocity (U/U_∞) behind upstream cylinders 1 and 2, and downstream cylinders 3 and 4. At $L/D = 1.5$, the mean transverse velocity distributions also suggest that the flow structure behind the downstream cylinders is distinctly biased to one side at the positions of $x/D = 2.25$ and $x/D = 4.25$, and begin to amalgamate at the position of $x/D = 6.25$ (refer to Fig. 4a). At $L/D = 3.5$, the mean transverse

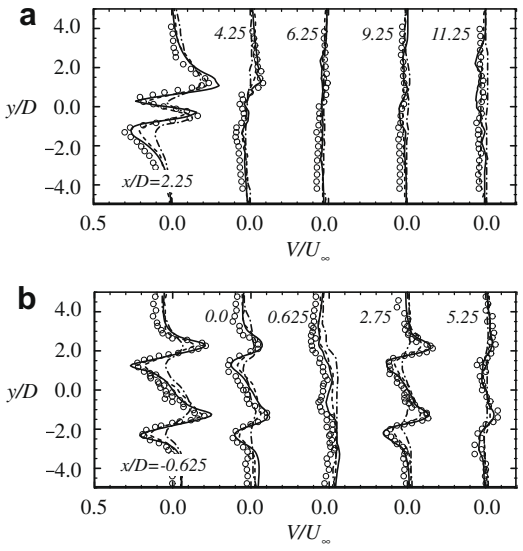

Fig. 4. Comparison of the mean transverse velocity distributions derived from LDA measurements at different x-positions at $Re = 15{,}000$: (a) $L/D = 1.5$ and (b) $L/D = 3.5$; The LDA results: (○), dash dot line: LES results with grid Model-A, dashed line: LES results with grid Model-B, solid line: LES results with grid Model-C.

velocity distributions also suggest that the vortex shedding from the upstream cylinders occurs at the position of $x/D = -0.625$ (refer to Fig. 4b). The mean transverse velocity distribution at the position of $x/D = 0.625$ behaves relatively calmer than that at the position of $x/D = 2.25$. It may be attributed to that the downstream cylinders were impinged by oncoming vortices and the shear layers of the downstream cylinders were pushed so as to roll up at further downstream positions.

Furthermore, the present LES results of both the mean streamwise and transverse velocity distributions agree quite well with those by LDA measurements at $Re = 15{,}000$ with $L/D = 1.5$ and 3.5, respectively, when adopting the grid Model-C (see Table 1, Figs. 3a and c and 4). For the different grid models, it can be seen that the difference of the results between the grid Model-B and grid Model-C is very small except when using grid Model-A. From these comparisons, it is quite confident that the LES model with grid Model-C will be sufficient to replicate and predict the complex turbulent flow characteristics of the four in-line cylinders configuration. Therefore, the three-dimensional numerical simulations can be used to reveal more information which cannot be obtained easily through experimental measurements.

4.2. Force characteristics and Strouhal numbers

Table 2 shows the present LES simulation results of the mean drag coefficients $\overline{C}_{D1}, \overline{C}_{D2}, \overline{C}_{D3}$ and $\overline{C}_{D4}$ (subscripts 1–4 refer to the upstream cylinders and downstream cylinders, respectively), the root mean square fluctuating lift coefficients $C'_{L1}, C'_{L2}, C'_{L3}$ and $C'_{L4}$and the corresponding Strouhal number ($St = f_s D/U_\infty$, f_s is the vortex-shedding frequency) for cylinders compared with the experimental results by Sayers (1990), Lam and Fang (1995) and Lam et al. (2003b). In general, there are only some small disparities between the present results and those obtained from experiments as there are also some differences among the experimental results. It may be due to the effects related to the differences in Reynolds number, spacing ratio, blockage ratio, ambient turbulence etc. It should be noted that the values of $\overline{C}_{D4}$ and C'_{L4} differ from those of $\overline{C}_{D3}$ and C'_{L3} when the spacing ratio of $L/D = 1.5$. It is another manifestation on the difference in formation length and wake width behind the downstream cylinder 3 and 4 (see Fig. 3a).

Table 2
Experimental and computational results on *St*, mean drag and fluctuating lift coefficients of four cylinders in an in-line square configuration.

Authors	*L/D*	*Re*	$\overline{C}_{D1}$	$\overline{C}_{D2}$	$\overline{C}_{D3}$	$\overline{C}_{D4}$	$\overline{C}'_{L1}$	$\overline{C}'_{L2}$	$\overline{C}'_{L3}$	$\overline{C}'_{L4}$	St_1	St_2	St_3	St_4
Sayers (1990) exp.	1.5	30,000	1.21			−0.13					0.124			0.103
H/D = 11.6	4.0		1.27			0.38					0.186			0.177
Lam and Fang (1995) exp.	1.56	12,800	1.19	1.24	−0.29	−0.37								
H/D = 28.4	3.58		1.35	1.36	0.59	0.59								
Lam et al. (2003b) exp.	1.69	41,000	1.40			−0.20	0.11			0.19				0.22
H/D = 17	3.4		1.19			0.25	0.06			0.38			0.20	0.16
Present 3D LES	1.5	15,000	1.36	1.35	−0.23	−0.19	0.10	0.06	0.28	0.34			0.125	0.169
	3.5		1.28	1.27	0.70	0.69	0.66	0.62	1.22	1.25	0.196	0.192	0.192	0.196

Referring to the results of Strouhal numbers obtained by the LES method, with the spacing ratio of *L/D* = 1.5, it is observed that no vortex shedding behind the upstream cylinders 1 and 2 can be found while the shedding frequency between the downstream cylinders 3 and 4 are much different (see Table 2). It is important to realize that the deflected wake feature evolves behind the downstream cylinders and dominates the flow characteristics. A narrow wake of high vortex-shedding frequency and a wide wake of low vortex-shedding frequency were obtained. It is also in agreement with the flow patterns shown by Lam and Lo (1992). With the spacing ratio of *L/D* = 3.5, however, the vortex shedding appears behind both the upstream and downstream cylinders and the near wake of the upstream cylinders 1 and 2 is not stable. The wake is seen to be slightly deflected from the streamwise direction. In general, the Strouhal numbers for all cylinders are all slightly less than 0.2 at *L/D* = 3.5. The present LES results of force characteristics highlight the dependence of vortex-shedding characteristics on the change of flow patterns.

4.3. Typical flow patterns with L/D = 1.5 and 3.5

Fig. 5 shows the instantaneous spanwise vorticity field and velocity field measured by DPIV with the spacing ratio of *L/D* = 1.5 at the Reynolds numbers from 11,000 to 20,000. It can be seen that, referring to the Strouhal number characteristics, the free shear layers from the upstream cylinders shield the corresponding downstream cylinders completely at all of the Reynolds numbers in the present study. It shows a bistable flow pattern behind the downstream cylinders. The wake structure is similar to that observed for *L/D* = 1.54 and *Re* = 2100 by Lam and Lo (1992).

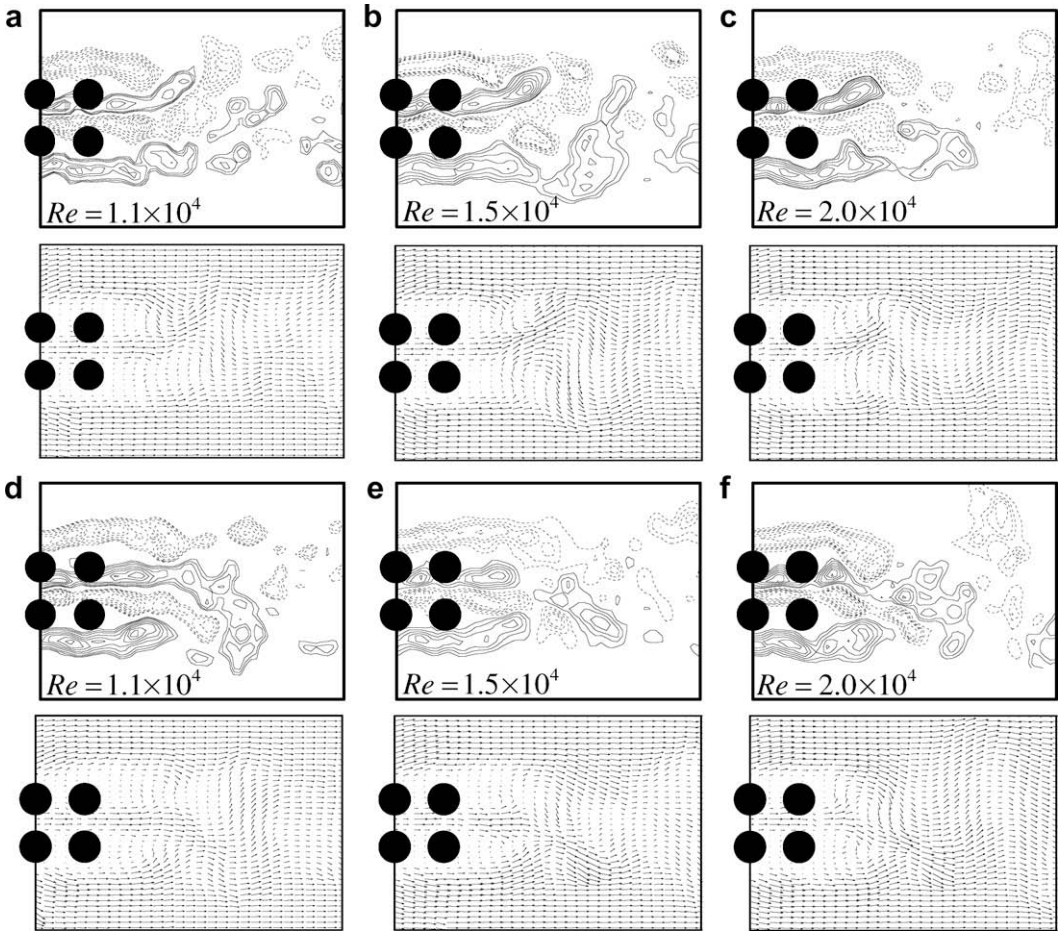

Fig. 5. Instantaneous vorticity field and velocity field derived from DPIV measurements at *L/D* = 1.5 for *Re* = 11,000, 15,000 and 20,000. Dashed and solid lines correspond to negative and positive vorticity, respectively.

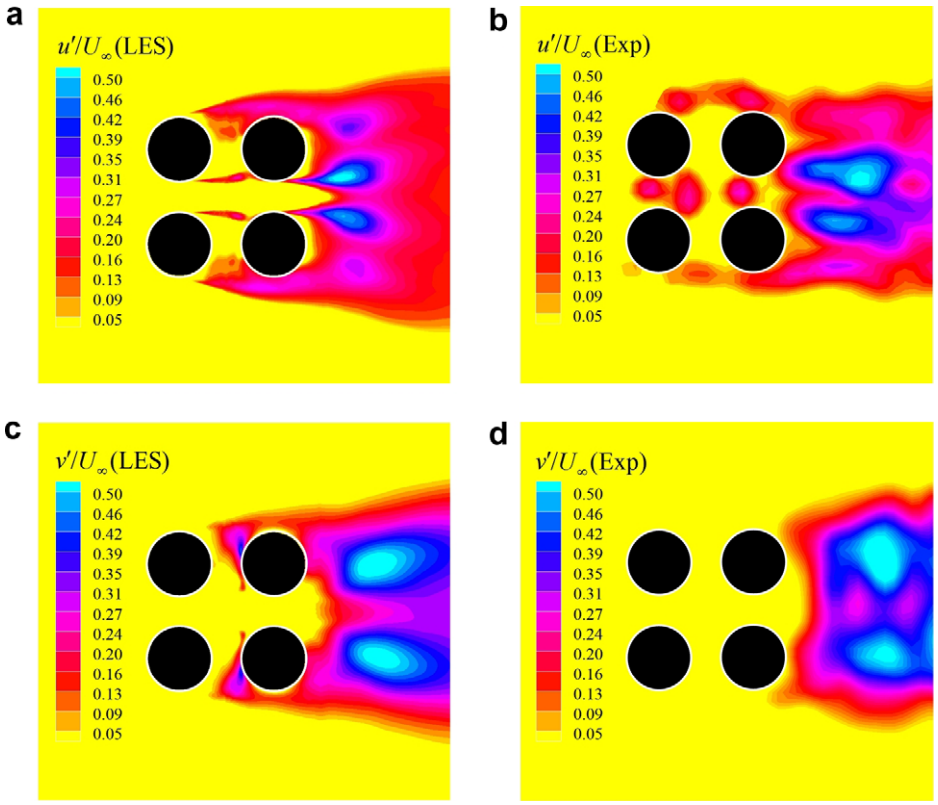

Fig. 6. Normalized time-averaged streamwise and transverse fluctuating velocity fields derived from DPIV measurements and LES simulations at $L/D = 1.5$ for $Re = 15{,}000$.

The intermittent change of the wide and narrow wakes behind the downstream cylinders was also observed at each Reynolds numbers. However, this bistable nature of the wake flow appears to occur randomly with upward deflection or downward deflection. The wake dynamics associated with the amalgamation and the coalescent effect of the vortices behind the downstream cylinders at this configuration are clearly demonstrated. It should be noted that the deflection angle (the angle of the main near wake velocity vectors based on the wake central line behind the downstream cylinders in the streamwise direction) of the wake structure behind the downstream cylinders also appears to be sensitive to the variation of Reynolds numbers and the sensitivity decreases as *Re* increases. This phenomenon of wake characteristics is strongly supported by the results obtained from LDA and LES results as shown in Fig. 3a and Fig. 4. Fig. 6 presents that normalized time-averaged root mean square contours distributions in the *x*–*y* plane of the fluctuating streamwise velocity (u'/U_∞) and the transverse velocity (v'/U_∞) derived from DPIV for the four cylinders case at the spacing ratio of $L/D = 1.5$ and $Re = 15{,}000$ compared with the LES results. The contours of the fluctuating streamwise velocity (u'/U_∞) with asymmetric maximum value positions about the centreline axis of each downstream cylinder (cylinders 3 and 4) in the near wake can be easily observed for both the experimental and LES results. Similarly, the fluctuating streamwise velocity, the deflection distribution of the fluctuating transverse velocity (v'/U_∞) along the centreline axis of each downstream cylinder in the near wake can also be found (see Fig. 5c and d). It is caused by the deflected flow pattern with a narrow and wide wake behind the downstream cylinders. This characteristic also reflects the bistable flow characteristics discussed above.

At the critical spacing ratio region of $L/D = 3.5$, depending on the variation of Reynolds number, the two flow patterns could be identified in Fig. 7. Distinct vortex shedding of the upstream cylinders was suppressed for $L/D = 3.5$ at $Re = 11{,}000$. The shear layer of the upstream cylinders rolled up very near the frontal part of the downstream cylinders and vortices are shed immediately downstream of cylinders 3 and 4 because of the combined effect of the shear layer of the upstream cylinders (see Fig. 7a). At $Re = 15{,}000$ and 20,000, the separated shear layer rolled up into vortices alternatively behind the upstream cylinders, the downstream cylinders were immersed the wake of the upstream cylinders and impinged by the oncoming vortices. It is expected that the fluctuating forces on the downstream cylinders are greater than those acting on the upstream cylinders due to the impingement of the vortices from the upstream cylinder (see Table 2). The flow behaviour such as in-phase vortex shedding, anti-phase vortex shedding and synchronized vortex shedding from the upstream cylinders was also observed using the DPIV technique (see Fig. 7b and c). Fig. 8 shows the normalized mean streamwise velocity (U/U_∞) and normalized root mean square values of the fluctuating streamwise velocity (u'/U_∞) along the $y/D = 1.75$ plane (the centreline plane behind the tandem cylinders 2 and 3) with $L/D = 3.5$ at $Re = 11{,}000$, 15,000 and 20,000, respectively. The LES results for $L/D = 3.5$ at $Re = 15{,}000$ is also added for comparison and also demonstrated good agreement with the experimental measurements. It indicates again that the flow pattern transformation around the four cylinders depends on the effect of Reynolds numbers at the critical spacing ratio region of $L/D = 3.5$. It can also be seen that the vortex formation length for the upstream cylinders decreases as *Re* decreases. There is a decrease of about 16% in the vortex formation length for the upstream cylinders as *Re* increases from 15,000 to 20,000.

Fig. 9 shows the instantaneous velocity fields over the iso-vorticity surfaces of the spanwise vorticity for the four cylinders configurations with the spacing ratio of $L/D = 1.5$ and 3.5 at $Re = 15{,}000$, respectively. The complex three-dimensional vortex

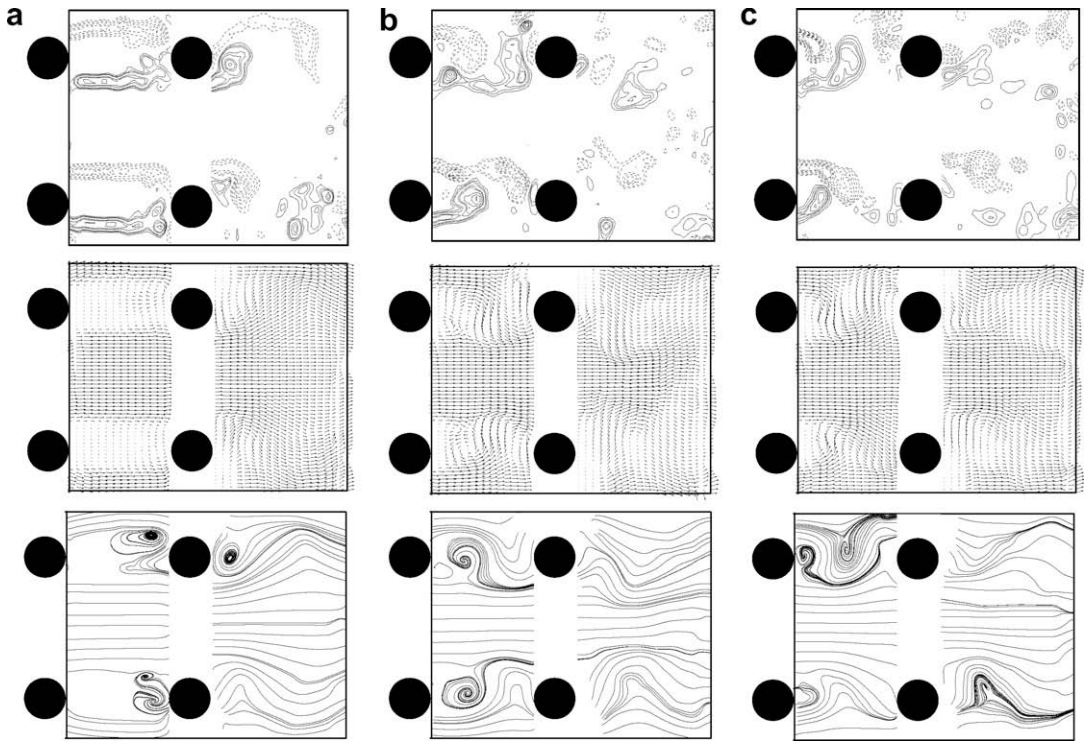

Fig. 7. Instantaneous vorticity fields, velocity fields and streamlines derived from DPIV measurements at $L/D = 3.5$: (a) $Re = 11{,}000$, (b) $Re = 15{,}000$ and (c) $Re = 20{,}000$. Dashed and solid lines correspond to negative and positive vorticity, respectively.

structures behind the downstream cylinders of the different biased flows for the $L/D = 1.5$ case were captured (see Fig. 9a and b). The upward deflected downstream wake structures and the downward deflected wake structures show good qualitative agreement with the observed flow visualization results derived from DPIV at the same Reynolds number (see Fig. 5b and e). It can be observed that the free shear layers from the upstream cylinders covered the corresponding downstream cylinders completely. Also as shown in Fig. 9c and d, the three-dimensional wake structures between the four cylinders in the anti-phase vortex shedding and in-phase vortex shedding with the spacing ratio of $L/D = 3.5$ are same with those DPIV visualization results (see Fig. 7b) and the free shear layers from upstream cylinders roll up into mature vortices and impinge on the downstream cylinder surfaces, which consist with the velocity distributions plots at the same Reynolds number and spacing ratio in Figs. 3 and 4.

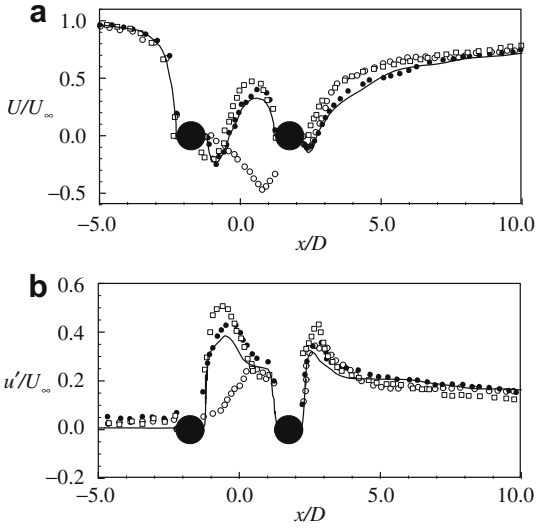

Fig. 8. LDA measurements and LES results along the x–z plane ($y/D = 1.75$) for $L/D = 3.5$: (a) mean streamwise velocity and (b) fluctuating streamwise velocity. LDA results: (○) $Re = 11{,}000$, (●) $Re = 15{,}000$ and (□) $Re = 20{,}000$; the solid line: LES results at $Re = 15{,}000$.

4.4. Reynolds stresses

Fig. 10 shows the distributions of the normalized shear stresses $\langle u'v' \rangle / U_\infty^2$ and the normalized longitudinal Reynolds stresses $\langle u'u' \rangle / U_\infty^2$ and the normalized transverse Reynolds stresses $\langle v'v' \rangle / U_\infty^2$ calculated by LES at different x/D positions with the spacing ratio of $L/D = 1.5$. The occurrence of the maximum centreline $\langle u'u' \rangle / U_\infty^2$ may be used to define the formation length of span-

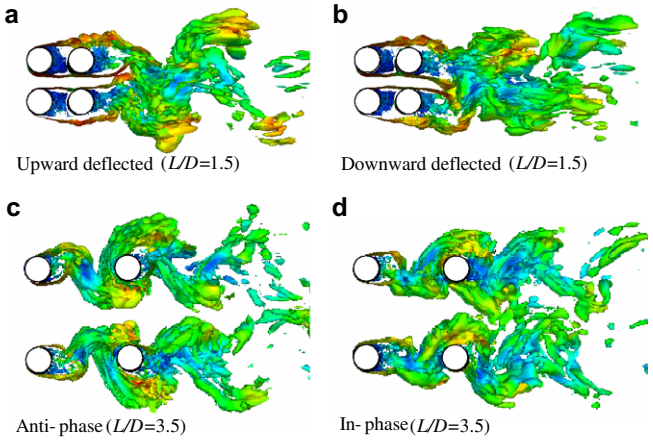

Fig. 9. LES results of velocity fields over the iso-vorticity surfaces for the four cylinders with $L/D = 1.5$ and 3.5 at $Re = 15{,}000$: (a) deflected upwards, (b) deflected downwards (c) anti-phase vortex shedding, (d) in-phase vortex shedding.

wise vortices (Bloor, 1964; Lam et al., 2004). The distributions of $\langle u'u'\rangle/U_\infty^2$ and $\langle v'v'\rangle/U_\infty^2$ exhibit asymmetry at $x/D = 2.25$ for $L/D = 1.5$ (see Fig. 10a and b). The double peaks of $\langle u'u'\rangle/U_\infty^2$ with different values behind each downstream cylinder indicate the two rows of alternating vortices with different vortex formation length occur behind each downstream cylinder. Furthermore, the distances between the double peaks of $\langle u'u'\rangle/U_\infty^2$ are about 0.75D and 0.65D behind the downstream cylinders 3 and 4, respectively. It suggests that the different wake width occurs behind the different downstream cylinders. The LDA and DPIV measurements and the LES simulations clearly display a deflect gap flow with a narrow and wide wake. The vortex streets become asymmetric with different vortices formation length behind the downstream cylinders at same spacing ratio. This asymmetric alternating vortex streets could lead to the asymmetric distributions of $\langle u'u'\rangle/U_\infty^2$ and $\langle v'v'\rangle/U_\infty^2$. The double peak of $\langle u'u'\rangle/U_\infty^2$ behind each downstream cylinder vanished after $x/D = 4.25$. It indicates the occurrence of vortex coalescence leading to wake amalgamation. The DPIV experiment also displays the wide wake dominates the narrow wake and deflects toward one side after $x/D = 4.25$ (see Fig. 5b and e). This could provide an explanation as to why a skew smaller single peak of $\langle u'u'\rangle/U_\infty^2$ and asymmetric larger value of $\langle v'v'\rangle/U_\infty^2$ behind each downstream cylinder occur at the position of $x/D = 4.25$. On the other hand, as shown in Fig. 10c, the value of $\langle u'v'\rangle/U_\infty^2$ is anti-symmetrical and may not be significantly affected by the asymmetry of the vortex streets. The Reynolds stress distributions at $x/D = 2.25$ is considerably greater due to the higher turbulent intensity near the cylinders.

With the spacing ratio of $L/D = 3.5$, as shown in Fig. 11, behind each of upstream and downstream cylinders, the $\langle u'u'\rangle/U_\infty^2$ displays a double peaks of almost equal value, the $\langle v'v'\rangle/U_\infty^2$ shows a single peak occurring at the $y/D = \pm 1.75$ planes and the $\langle u'v'\rangle/U_\infty^2$ shows an anti-symmetrical characteristic about $y/D = 0$. The maximum value of $\langle u'u'\rangle/U_\infty^2$, $\langle v'v'\rangle/U_\infty^2$ and $\langle u'v'\rangle/U_\infty^2$ all occur at the position of $x/D = -0.625$ and may imply the large-scale vertical motion of the vortex in corresponding sections of the wake. They are also consistent with the results obtained by DPIV experiments (see Fig. 7b).

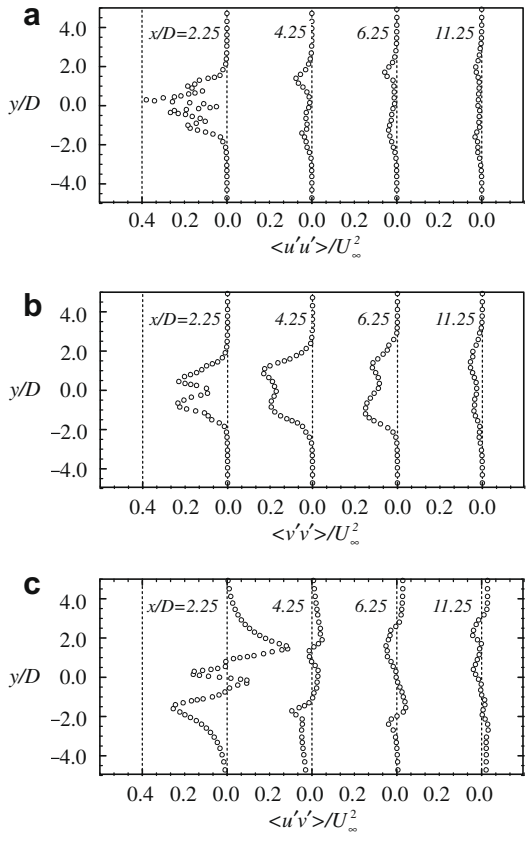

Fig. 10. Distributions of the normalized longitudinal Reynolds stresses $\langle u'u'\rangle/U_\infty^2$, the transverse Reynolds stresses $\langle v'v'\rangle/U_\infty^2$ and the shear stresses $\langle u'v'\rangle/U_\infty^2$ calculated by LES at different x-positions for $L/D = 1.5$ and $Re = 15{,}000$.

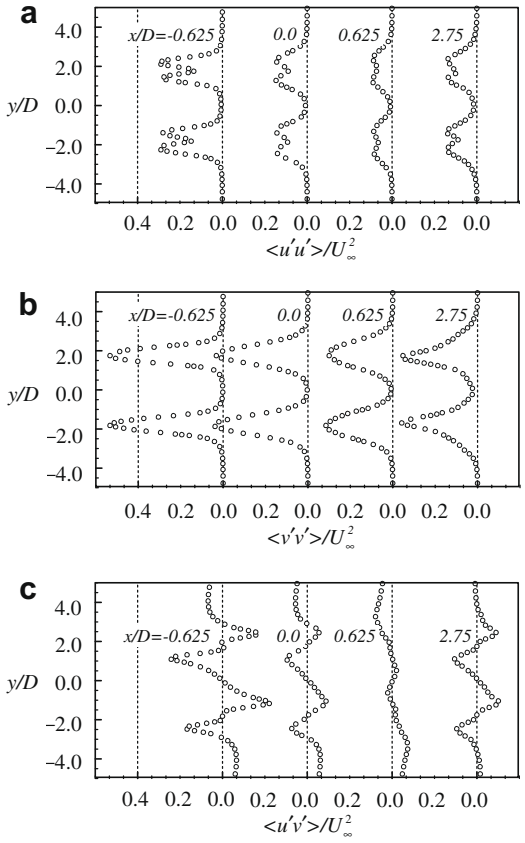

Fig. 11. Distributions of the normalized longitudinal Reynolds stresses $\langle u'u'\rangle/U_\infty^2$, the transverse Reynolds stresses $\langle v'v'\rangle/U_\infty^2$ and the shear stresses $\langle u'v'\rangle/U_\infty^2$ calculated by LES at different x-positions for $L/D = 3.5$ and $Re = 15{,}000$.

5. Conclusions

The turbulent flow around the four cylinders in an in-line square configuration with spacing ratios of $L/D = 1.5$–5.0 at subcritical Reynolds numbers from 11,000 to 20,000 are investigated using LDA and DPIV measurements. The three-dimensional numerical simulations were also performed using the large eddy simulation. Some valuable data such as, velocity distributions, 3D wake structures, drag and lift force characteristics and Reynolds stress, etc. were obtained.

Depending on the variation of the spacing ratios and Reynolds numbers, several distinct flow patterns were captured. With the spacing ratio of $L/D = 1.5$, the bistable flow nature was observed both in the experimental study and the numerical simulations. The biased flow deflection angle of the wake structure decreases with the increasing of Reynolds numbers. Symmetrical flow pattern occurs at higher spacing ratio ($L/D = 2.5$). The distinct vortex shedding from the upstream cylinders is suppressed for $L/D < 3.5$ at such subcritical Reynolds numbers. The vortex formation length for the upstream and downstream cylinders is affected by the spacing ratio and the Reynolds number. For the critical spacing ratio of $L/D = 3.5$, there is a decrease of about 16% in the vortex formation

length for the upstream cylinders as *Re* increases from 15,000 to 20,000. Both the symmetrical (anti-phase) and anti-symmetrical (in-phase) wake patterns were observed at $L/D = 3.5$. As the spacing ratio further increases to $L/D = 5.0$, the symmetrical flow pattern occurs again. Moreover, the flow patterns of the turbulent flow around the four cylinders have an essential influence on the forces distributions. Analysis of the calculated Reynolds stress shows that the deflected vortex streets could give rise to the asymmetry of the values $\langle u'u' \rangle / U_\infty^2$ and $\langle v'v' \rangle / U_\infty^2$ for $L/D = 1.5$. While at spacing ratio $L/D = 3.5$, symmetrical distributions of Reynolds stress are captured.

Acknowledgement

The authors wish to thank the Research Grants Council of the Hong Kong Special Administrative Region, China, for its support through Grant No. PolyU 5299/03E.

References

Bloor, S., 1964. The transition to turbulence in the wake of a circular cylinder. Journal of Fluid Mechanics 19, 290.

Breuer, M., 1998. Large eddy simulation of the subcritical flow past a circular cylinder: numerical and modeling aspects. International Journal of Numerical Method in Fluids 28, 1281–1302.

Carmo, B.S., Meneghini, J.R., 2006. Numerical investigation of the flow around two circular cylinders in tandem. Journal of Fluids and Structures 22, 979–988.

Deng, J., Ren, A.L., Zou, F., Shao, X.M., 2006. Three-dimensional flow around two circular cylinders in tandem arrangement. Fluid Dynamics Research 38, 386–404.

Farrant, T., Tan, M., Price, W.G., 2000. A cell boundary element method applied to laminar vortex-shedding from arrays of cylinders in various arrangements. Journal of Fluids and Structures 14, 375–402.

Lam, K., Fang, X., 1995. The effect of interference of four equispaced cylinders in cross flow on pressure and force coefficients. Journal of Fluids and Structures 9, 195–214.

Lam, K., Lin, Y.F., 2008. Large eddy simulation of flow around wavy cylinders at a subcritical Reynolds number. International Journal of Heat and Fluid Flow 29, 1071–1088.

Lam, K., Lo, S.C., 1992. A visualization study of cross-flow around four cylinders in a square configuration. Journal of Fluids and Structures 6, 109–131.

Lam, K., Zou, L., 2006. The effects of aspect ratio and end condition on the control of free shear layers development and force coefficients for flow past four cylinders in the in-line square configuration. In: IUTAM Symposium on Flow Control and MEMS, 106 London, UK.

Lam, K., Li, J.Y., Chan, K.T., So, R.M.C., 2003a. Flow pattern and velocity field distribution of cross-flow around four cylinders in a square configuration at low Reynolds number. Journal of Fluids and Structures 17, 579–665.

Lam, K., Li, J.Y., So, R.M.C., 2003b. Force coefficient and Strouhal numbers of four cylinders in cross flow. Journal of Fluids and Structures 18, 305–324.

Lam, K., Wang, F.H., So, R.M.C., 2004. Three-dimensional nature of vortices in the near wake of a wavy cylinder. Journal of Fluids and Structures 19, 815–833.

Lam, K., Gong, W.Q., So, R.M.C., 2008. Numerical simulation of cross-flow around four cylinders in an in-line square configuration. Journal of Fluids and Structures 24, 34–57.

Ng, C.W., Cheng, V.S.Y., Ko, N.W.M., 1997. Numerical study of vortex interactions behind two circular cylinders in bistable flow regime. Fluid Dynamics Research 19, 379–409.

Norberg, C., 1998. LDV-measurements in the near wake of a circular cylinder. In: Proceedings of the 1998 ASME Fluids Engineering Division Summer Meeting, Washington, DC, FED-vol. 245, FEASM98-5202.

Park, C.W., Lee, S.J., 2003. Flow structure around two finite circular cylinders located in an atmospheric boundary layer: side-by-side arrangement. Journal of Fluids and Structures 17, 1043–1068.

Sayers, A.T., 1988. Flow interference between four equispaced cylinders when subjected to a cross flow. Journal of Wind Engineering and Industrial Aerodynamics 31, 9–28.

Sayers, A.T., 1990. Vortex shedding from groups of three and four equispaced cylinders situated in cross-flow. Journal of Wind Engineering and Industrial Aerodynamics 34, 213–221.

Sohankar, A., Davidson, L., Norberg, C., 2000. Large eddy simulation of flow past a square cylinder: comparison of different subgrid scale models. Journal of Fluids Engineering 122, 39–47.

Sumner, D., Price, S.J., Paidoussis, M.P., 2000. Flow-pattern identification for two staggered circular cylinders in cross-flow. Journal of Fluid Mechanics 411, 263–303.

Wang, Z.J., Zhou, Y., 2005. Vortex interactions in a two side-by-side cylinder near wake. International Journal of Heat and Fluid Flow 26, 362–377.

Williamson, C.H.K., 1996. Vortex dynamics in the cylinder wake. Annual Review of Fluid Mechanics 28, 477–539.

Williamson, C.H.K., Wu, J., Sheridan, J., 1995. Scaling of streamwise vortices in wakes. Physics of Fluids 7, 2307–2309.